applied sciences

MDPI

Article

Convective Heat Transfer and Particle Motion in an Obstructed Duct with Two Side by Side Obstacles by Means of DPM Model

Saman Rashidi [1,†], Javad Aolfazli Esfahani [2,†] and Rahmat Ellahi [3,*,†]

1 Department of Mechanical Engineering, Semnan Branch, Islamic Azad University, Semnan, Iran; samanrashidi3983@gmail.com
2 Department of Mechanical Engineering, Ferdowsi University of Mashhad, Mashhad 91775-1111, Iran; abolfazl@um.ac.ir
3 Department of Mathematics & Statistics, FBAS, IIUI, Islamabad 44000, Pakistan
* Correspondence: rahmatellahi@yahoo.com; Tel.: +92-51-9019-510
† All authors contributed equally to this work.

Academic Editors: Yulong Ding and Yuyuan Zhao
Received: 11 January 2017; Accepted: 19 April 2017; Published: 24 April 2017

Abstract: In this research, a two-way coupling of discrete phase model is developed in order to track the discrete nature of aluminum oxide particles in an obstructed duct with two side-by-side obstacles. Finite volume method and trajectory analysis are simultaneously utilized to solve the equations for liquid and solid phases, respectively. The interactions between two phases are fully taken into account in the simulation by considering the Brownian, drag, gravity, and thermophoresis forces. The effects of space ratios between two obstacles and particle diameters on different parameters containing concentration and deposition of particles and Nusselt number are studied for the constant values of Reynolds number (Re = 100) and volume fractions of nanoparticles (Φ = 0.01). The obtained results indicate that the particles with smaller diameter (d_p = 30 nm) are not affected by the flow streamline and they diffuse through the streamlines. Moreover, the particle deposition enhances as the value of space ratio increases. A comparison between the experimental and numerical results is also provided with the existing literature as a limiting case of the reported problem and found in good agreement.

Keywords: concentration; deposition; two-way coupling; side-by-side obstacles; discrete phase model (DPM)

1. Introduction

Investigations of the momentum and heat transfer specifications in an obstructed duct with multiple obstacles has many thermal applications including compact heat exchangers, flow around arrays of nuclear fuel rods, cooling of electronic devices, oil or gas flows in reservoirs, chimney stacks, power generators, etc. [1]. The heat transfer improvement in all mentioned applications is an essential need. Nanofluids are recognized as high heat transfer performance fluids, which can be used in many cooling systems including cooling of electronic components, oil coolers, inter coolers, and coolant in microchannel heat sink [2,3]. The particulate fouling as a destructive phenomenon in nanofluids should be taken into consideration as it can affect the favorable improved thermal properties of these fluids. Accurate understanding of the particle motion is essential to supress the destructive effects of this phenomenon.

In past years, researchers used different models for simulating nanofluid flow for different problems. These models are single-phase approach, Eulerian model, volume of fluid model, mixture

model, and Eulerian–Lagrangian approach (Discrete phase model). Vanaki et al. [4] reviewed these models. They concluded that the Eulerian-Lagrangian approach is more precise and reliable for simulating the nanofluid because it takes into account the interactions between two phases by considering the Brownian, drag, gravity, and thermophoresis forces between them. Moreover, this model has ability to predict particle distribution and calculate concentration of nanoparticles in domain. He et al. [5] performed a comparison between single-phase and Lagrangian trajectory approaches for simulating the nanofluid flow in a tube. They found that the Lagrangian trajectory approach predicts a higher heat transfer coefficient in comparison with the single-phase one as the Lagrangian trajectory approach considers the dynamic of particles and the interactions between liquid and particulate phases. Mirzaei et al. [6] used the Eulerian–Lagrangian approach to investigate the nanofluid flow in a microchannel. They reported the same findings about the greater prediction of heat transfer coefficient by this model in comparison to the single-phase one. In another study, Bahremand et al. [7] studied the nanofluid turbulent flow in helically-coiled tubes. They used the Eulerian-Lagrangian approach. Besides the numerical study, they performed an experimental work on this problem to benchmark the accuracy of the numerical model. They observed that the Eulerian–Lagrangian model presents the results with higher accuracy in comparison to the single-phase one. Some researchers studied the flow and heat transfer in an obstructed channel. Turki et al. [8] studied the convective heat transfer across an obstructed duct with a built-in heated square obstacle. Their results indicated that the Strouhal number increases with an enhance in the Richardson number. Mohammadi Pirouz et al. [9] simulated the heat exchange in a duct with wall-mounted square obstacles. They reported that the flow accelerates near faces with a decrease in the distance between obstacles. This leads to enhance in the heat transfer rate from obstacles. Heidary and Kermani [10] investigated the influences of nanofluid on heat transfer improvement in an obstructed duct. They applied the single-phase approach for modelling the nanofluid for this problem. They observed about 60% enhancement for heat transfer in the duct by using the nanoparticles and the blocks. Readers are referred to the most significant studies on nanoparticles in [11–20] and several references therein. Recently, Shahmohamadi and Rashidi [21] analytically studied how nanofluids flow through a rotating channel with a lower stretching porous wall under the influence of a magnetic field. They reported that the nanoparticle additives have considerable influence on the flow. In other research, Shahmohamadi et al. [22] investigated tribological performance of carbon nanoparticles dispersed in polyalphaolefin PAO6 oil. They concluded that the presence of nanoparticles causes a higher lubricant viscosity.

Previous researchers concluded that the Eulerian–Lagrangian model (Discrete phase model) is a superior model to simulate the nanofluid, as it can predict particle distribution and calculate concentration and deposition of nanoparticles in the domain. Enhancement of heat transfer is a very important problem for an obstructed duct with multiple obstacles as it has many thermal applications such as compact heat exchangers. Nanofluids can be introduced as an option to achieve this target. The particulate fouling phenomenon in nanofluids should be taken into consideration as it can affect the favorable improved thermal properties of these fluids. This paper simulates the convective heat transfer and particle motion and deposition in an obstructed duct with two side-by-side obstacles by a two-way coupling of DPM model. The present research represents the first study about the application of two-way coupling of DPM model to simulate nanofluid in this geometry.

2. Formulation of the Problem

2.1. Physical Characteristic

A view of the computational domain is disclosed in Figure 1. A two-dimensional obstructed duct with two side-by-side obstacles is modelled. Computational domain is subjected to a free stream with parabolic speed and uniform temperature (T_h = 310 K). It is assumed that the stream is incompressible, time dependent, and laminar. The obstacles and duct walls are kept at constant temperature (T_c = 300 K). Two side-by-side obstacles with sides D are mounted in the duct. S is the

gap between the centers of the obstacles. The upstream and downstream lengths of the duct are fixed as 30*D* and 60*D*, respectively. The duct height is considered to be 16*D*. The gravity is in the stream-wise direction.

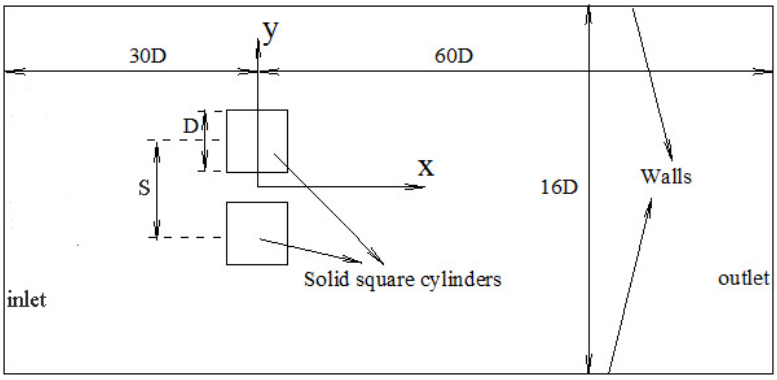

Figure 1. Computational domain and coordinate system.

The interactions between the liquid and aluminum oxide particles are taken into account for the simulations. Moreover, the collisions between particles are ignored. Note that for particles in the range of nanometer with low values of volume fraction, the chances that any two random particles would be close enough to interact with each other are extremely low [23]. Accordingly, the interactions between the particles in the range of nanometer can be ignored. However, for particles with higher diameter (e.g., 0.5 μm), it is better to consider the effects of particle-particle interactions. It should be stated that in DPM, it is not possible to track all physical particles. Instead, representative particles or parcels should be tracked. Any parcel is representative of specified number of actual particles with the same physical property, which is characterized by the particle flow rate along each calculated particle trajectory. 5000 parcels [24] are assumed at $\Phi = 0.01$ for this research. Finally, it should be stated that all simulations are performed for the fixed values of Reynolds number ($Re = 100$) and volume fractions of nanoparticles ($\Phi = 0.01$) at variable particle diameter (30 nm–0.5 μm) and space ratio ($S/D = 1.5$–4.5).

2.2. Governing Equations

For two-way coupling of Eulerian-Lagrangian approach, the liquid phase is treated as a continuum by using the Eulerian approach, while the dispersed particles can be tracked by applying a Lagrangian approach. The heat, mass, and momentum can be exchanged between two phases [25,26]. The equations for two phases are presented separately as follows:

2.2.1. Liquid Phase

- Mass conservation equation:

$$\frac{\partial u}{\partial x} + \frac{\partial v}{\partial y} = 0 \tag{1}$$

where x and y are Cartesian coordinate components. Moreover, u and v are velocity components in x and y directions, respectively.

- Momentum equation:

$$\rho\left(\frac{\partial u}{\partial t} + u\frac{\partial u}{\partial x} + v\frac{\partial u}{\partial y}\right) = -\frac{\partial p}{\partial x} + \mu\left(\frac{\partial^2 u}{\partial x^2} + \frac{\partial^2 u}{\partial y^2}\right) + S_{vx} \tag{2}$$

$$\rho\left(\frac{\partial v}{\partial t} + u\frac{\partial v}{\partial x} + v\frac{\partial v}{\partial y}\right) = -\frac{\partial p}{\partial y} + \mu\left(\frac{\partial^2 v}{\partial x^2} + \frac{\partial^2 v}{\partial y^2}\right) + S_{vy} \tag{3}$$

where ρ, μ, p, and t are density of water, viscosity of water, pressure, and time, respectively.

- Energy equation:

$$\rho C_p\left(\frac{\partial T}{\partial t}+u\frac{\partial T}{\partial x}+v\frac{\partial T}{\partial y}\right)=k\left(\frac{\partial^2 T}{\partial x^2}+\frac{\partial^2 T}{\partial y^2}\right)+S_h \tag{4}$$

where C_p, k, and T are heat capacity of water, heat conductivity of water, and temperature, respectively. Moreover, the terms of S_v and S_h show the momentum and heat exchanges between two phases, respectively, and can be defined as [27,28]

$$S_v=\sum_{np}-\frac{m_p}{\delta V}\frac{d\,V_p}{dt} \tag{5}$$

$$S_h=\sum_{np}\frac{m_p}{\delta V}C_p\frac{dT_p}{dt} \tag{6}$$

where parameters with subscript of "p" are related to the particle phase. Accordingly, m_p, n_p, and δV are the particle mass, the number of particles in a cell volume, and the cell volume, respectively.

2.2.2. Particle Phase

For each particle suspended in the liquid, a differential form of force balance equation is utilized to obtain the trajectory of solid phase. The interaction forces between fluid and solid phases contain the drag, Brownian, gravity, and thermophoresis forces. The dynamic equations of solid phase are

$$\frac{dX_p}{dt}=V_p \tag{7}$$

$$\frac{dV_p}{dt}=\underbrace{\frac{18\mu_f}{d_p^2\rho_p C_c}(V_f-V_p)}_{\text{Drag force}}+\underbrace{\frac{g(\rho_p-\rho_f)}{\rho_p}}_{\text{Gravitational force}}+\underbrace{\varsigma\sqrt{\frac{\pi S_0}{\Delta t}}}_{\text{Brownian force}}\underbrace{-\frac{36\mu^2 C_s(k_f/k_p+C_t+Kn)}{\rho_f\rho_p d_p^2(1+3C_mKn)(1+2k_f/k_p+2C_tKn)}\frac{\nabla T}{T}}_{\text{Thermophoretic force}} \tag{8}$$

where subscripts of "f" and "p" demonstrate the liquid and solid phases, respectively. X and V indicate the location and velocity of the particles, respectively. Moreover, g, k, t, ρ, and μ are gravitational acceleration, heat conductivity, time, density, and viscosity, respectively.

C_c in drag force term denotes the Cunningham correction and is determined by

$$C_c=1+\frac{2\lambda}{d_p}\left[1.257+0.4e^{-(1.1d/2\lambda)}\right] \tag{9}$$

where d_p and λ are the particle diameter and fluid mean free path, respectively. Moreover, Kn in thermophoresis force terms is the Knudsen number. The constant values of C_m, C_t, and C_s, are respectively allocated as 1.14, 2.18, and 1.17 [29]. ς in Brownian force is the zero-mean, unit-variance independent Gaussian random numbers. Finally, S_0 is the spectral intensity of Brownian force and is calculated as follows [30,31]:

$$S_0=\frac{216\nu K_B T_f}{\pi^2\rho_f d_p^5\left(\frac{\rho_p}{\rho_f}\right)^2 C_c} \tag{10}$$

where K_B is the Boltzmann constant (=1.38 $\times$ 10^{-23} J K^{-1}).

The energy equation for the solid phase is presented as

$$m_p C_p\left(\frac{dT_p}{dt}\right)=hA_p(T_f-T_p) \tag{11}$$

where A_p is the particle surface area. Moreover, h is the heat transfer coefficient and is defined by [32]:

$$h = \frac{k_f}{d_p}\left(2 + 0.6Re_p^{0.5}Pr_f^{0.3}\right) \tag{12}$$

where Pr_f and Re_p are the Prandtl number of the liquid phase and particle Reynolds number, respectively.

3. Boundary Conditions

3.1. Liquid Phase

At the entrance of the duct, a parabolic velocity and a uniform temperature are used for velocity and temperature fields, respectively. Accordingly, the boundary condition at this section is defined by

$$u = U_0(1 - (2y/D)^2),\ v = 0, T = T_h \tag{13}$$

where U_0 is the velocity at the center of the duct.

Along the surfaces of the duct and obstacles, no-slip condition and constant temperature are considered for velocity and temperature fields, respectively. The boundary conditions for these regions are expressed by

$$u = 0,\ v = 0,\ T = T_c \tag{14}$$

At exit of the duct, zero gradient boundary conditions are used for both velocity and temperature fields. The boundary conditions for this section are expressed by

$$\frac{\partial u}{\partial x} = 0,\ \frac{\partial v}{\partial x} = 0,\ \frac{\partial T}{\partial x} = 0 \tag{15}$$

Eventually, it is supposed that there is no flow across the duct and the temperature is constant at initial time. This condition can be introduced by

$$u = 0,\ v = 0,\ T = T_h \tag{16}$$

3.2. Solid Phase

In this research, the escape boundary is considered at the entrance and exit sections of the duct. Based on this boundary, the trajectory computations are stopped when a particle exits from the domain. The temperature of particles in the entrance section is fixed at 310 K and the particle temperature drops to 300 K by colliding the particles with a surface. Eventually, the reflect boundary with a restitution coefficient of 1 is considered for all surfaces containing the surfaces of the duct and obstacle.

3.3. Physical Parameter

Physical parameters involved in this study are introduced in this section.

The local surface Nusselt number based on the channel width is calculated by

$$Nu = \frac{hH}{k_f} = \left.\frac{\partial T^*}{\partial n^*}\right|_{\text{on obstacle}} \tag{17}$$

where n and H are the normal direction to the channel walls and the width of the channel, respectively. Note that k_f in the above equation is the thermal conductivity of the fluid. Also, superscript "*" denotes the non-dimensional variables. T^* and n^* are defined by

$$T^* = \frac{T - T_c}{T_m - T_c},\ n^* = \frac{n}{H} \tag{18}$$

where T_c is the temperature on the walls of the duct. Moreover, T_m is mean temperature, defined by

$$T_m = \frac{1}{Hu_m} \int_{-\frac{H}{2}}^{+\frac{H}{2}} uTdy \tag{19}$$

where u_m is the mean velocity, calculated by

$$u_m = \frac{1}{H} \int_{-\frac{H}{2}}^{+\frac{H}{2}} udy \tag{20}$$

The heat flux can be evaluated by

$$q''_{\text{on the wall}} = h(T_m - T_c) = k_f \frac{\partial T}{\partial n} \tag{21}$$

Surface-mean Nusselt number is calculated by

$$\overline{Nu} = \frac{1}{A} \int_A NudA \tag{22}$$

where A indicates the surface of the duct. Finally, the time-mean Nusselt number is calculated as

$$\langle \overline{Nu} \rangle = \frac{1}{t} \int_0^t \overline{Nu} dt \tag{23}$$

where t is the time duration.

3.4. Definitions

The following concepts are used in this research:

Reflect boundary condition: This type of boundary usually used as particle boundary condition at wall, symmetry, and axis boundaries [33]. It should be stated that the particle rebounds off of the boundary in regard with a variation in its momentum as specified by the coefficient of restitution. Coefficient of restitution is defined by

$$\text{Coefficient of restitution} = \frac{V_{2,n}}{V_{1,n}} \tag{24}$$

where $V_{1,n}$ and $V_{2,n}$ are the particle velocities before and after particle-wall collision. This boundary has a restitution coefficient of 1.

Trap boundary condition: This type of boundary usually used as particle boundary condition at wall boundaries [33]. The trajectory calculations are terminated and the destiny of the particle is saved as trapped. This boundary has a restitution coefficient of 0.

Escape boundary condition: This type of boundary usually used as a particle boundary condition at all flow boundaries containing pressure and velocity inlets, pressure outlets, etc. [33]. The particle is considered as having "escaped" when it collisions the boundary in question. Trajectory calculations terminate for this type of boundary.

Deposition: The deposition is defined as the ratio of the number of deposited (trapped) particles on all involved surfaces containing obstacle and duct surfaces to the number of particles injected to the duct at specific time.

Concentration (Solid volume fraction): The void fraction of each cell in discrete particle model can be determined by

$$\varepsilon = 1 - \frac{\sum V_i}{\Delta V} \tag{25}$$

where V_i is the volume of ith particle in the cell. Moreover, the summation is taken over all the particles in the cell volume $\Delta V = \Delta x \Delta y d_p$. This means that the two-dimensional domain is regarded as a pseudo three-dimensional one with a thickness of one particle diameter d_p [34].

Parcel: In DPM, it is not possible to track all physical particles. Instead, representative particles or parcels should be tracked. A particle in each parcel is representative of the entire particles on that parcel and motion and heat exchange equations are solved only for this particle and extended to others. After solving the equations for particle, a Gaussian distribution function is used to make the connection between the particle and parcel parameters with

$$\theta_{parcel} = \sum N_{particle} G_w \theta_{particle} \tag{26}$$

$$G_w = \left(\frac{a}{\pi}\right)^{\frac{3}{2}} \exp\left(-a \frac{\left|x_{prcel} - x_{particle}\right|^2}{\Delta x^2}\right) \tag{27}$$

where θ is particle or parcel variable. G_w and N denote the Gaussian function and number of particles.

4. Numerical Results and Discussion

In the current computation, a finite volume method is utilized to discretize the equations of liquid and solid phases. Moreover, the pressure and velocity terms are stored at node center and node faces, respectively by using the staggered grid arrangement. The coupling between the pressure and velocity terms is achieved by SIMPLE algorithm of Patankar [35]. For using SIMPLE algorithm, the mass conservation and momentum equations for fluid are combined to drive the pressure-correction equation. The convection, diffusion, and time terms are discretized by applying a first order upwind scheme, a central difference algorithm, and a first order implicit method, respectively. Finally, the convergence is passed when the values of residuals reduced to $\leq 10^{-4}$ for all equations except the energy equation. This considered value is set at 10^{-6} for energy equation. All simulations are performed by the commercial software Ansys-Fluent. Figure 2 shows the procedure of the numerical solution in Fluent for this problem.

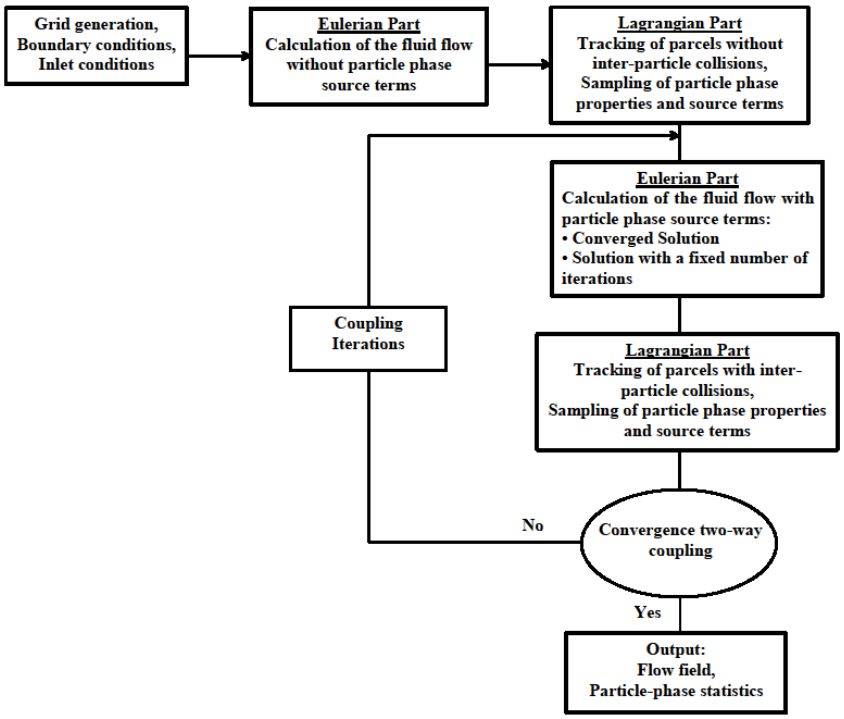

Figure 2. Procedure of numerical solution in Fluent for this problem.

4.1. Grid Study and Validation

A non-uniform square mesh is generated throughout the domain with a more density around the obstacles surfaces. A schematic view of this mesh with a near zone around the obstacles is disclosed in Figure 3. Various mesh sizes are explored to certify the sensitivity of the numerical outputs to the mesh resolution. The results of this test for the mean Nusselt number on the top wall of the duct at Re = 100, S/D = 1.5, d_p = 30 nm, and Φ = 0.01 are presented in Table 1. Note that δ/D in this table indicates the ratio of smallest cell size (δ) to side of the obstacle (D). It is observed that the difference in the mean Nusselt number between Cases 3 and 4 is 0.23%. Hence, the cell number of Case 3 is selected for the subsequent calculations.

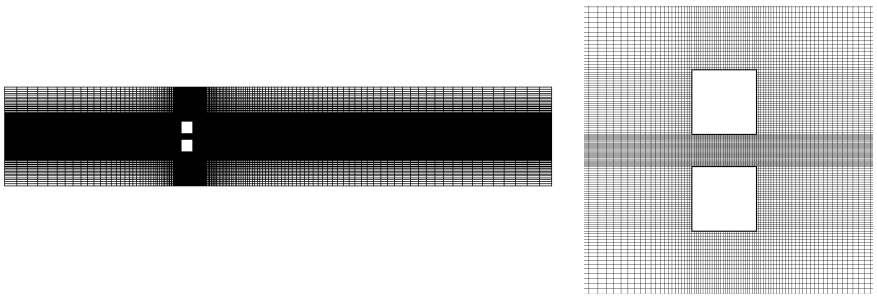

(**a**) (**b**)

Figure 3. Mesh distribution (**a**) whole domain (**b**) near the obstacles.

Table 1. The grid study at Re = 100, S/D = 1.5, d_p = 30 nm, and Φ = 0.01.

No.	Grid Number	δ/D	$\langle \overline{Nu} \rangle$	Percentage Difference
1	2375	0.05	3.342	1.34%
2	4750	0.033	3.387	1.01%
3	9500	0.025	3.421	0.23%
4	19,000	0.02	3.429	—

To examine the accuracy of the numerical results, the numerical outputs are benchmarked with experimental results obtained by Heyhat et al. [36]. The case for validation is aluminum oxide-water nanofluid flow with dp = 40 nm and Φ = 0.01 in a straight tube. The results of comparison between the experimental and numerical results are presented in Figure 4 for the variations of pressure drop ratio with Reynolds number. The pressure drop ratio is defined as the ratio of pressure drop of nanofluid to that of pure water. This comparison showed good agreement between the experimental and numerical results with a relative error about 5%.

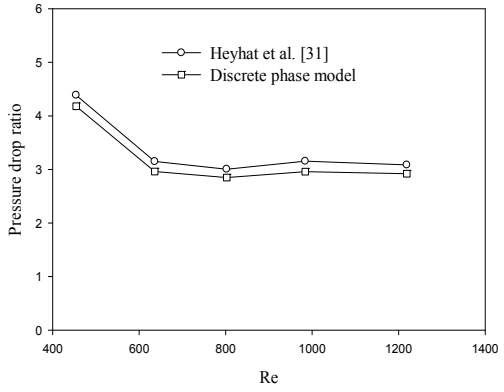

Figure 4. The ratio of pressure drop for Al_2O_3-water nanofluid versus Reynolds numbers at dp = 40 nm and Φ = 0.01.

4.2. Discussion

In this part, the results are discussed for various values of parameters containing the space ratio and particle diameter.

The particle dispersions inside the duct for different particle diameters at Re = 100, Φ = 0.01, and S/D = 3.5 are shown in Figure 5. This figure shows the locations of injected particles at a specific time, which are superimposed on vorticity contours. It is observed that the particles with diameters of 30 nm are dispersed at entire of the duct. Brownian force generated between the liquid molecules and the suspended particles causes the randomized dispersion of the particles. This force is larger in comparison to the inertial forces for smaller values of particle diameter. The particles with smaller diameter (dp = 30 nm) are not affected by the flow streamline and they diffuse through the streamlines. However, the particles with larger diameters (i.e., 0.1 and 0.25 μm) accumulate in the vorticity regions around the perimeter of the vortices. It should be stated that the larger particles are under the influence of forces created by the vortices and vortical flow field. Finally, the inertia forces of particles dominate the centrifugal forces formed by the flow for the particles with diameter of 0.5 μm and this causes the exit of particles from the vortices path line and tends them toward the duct surfaces.

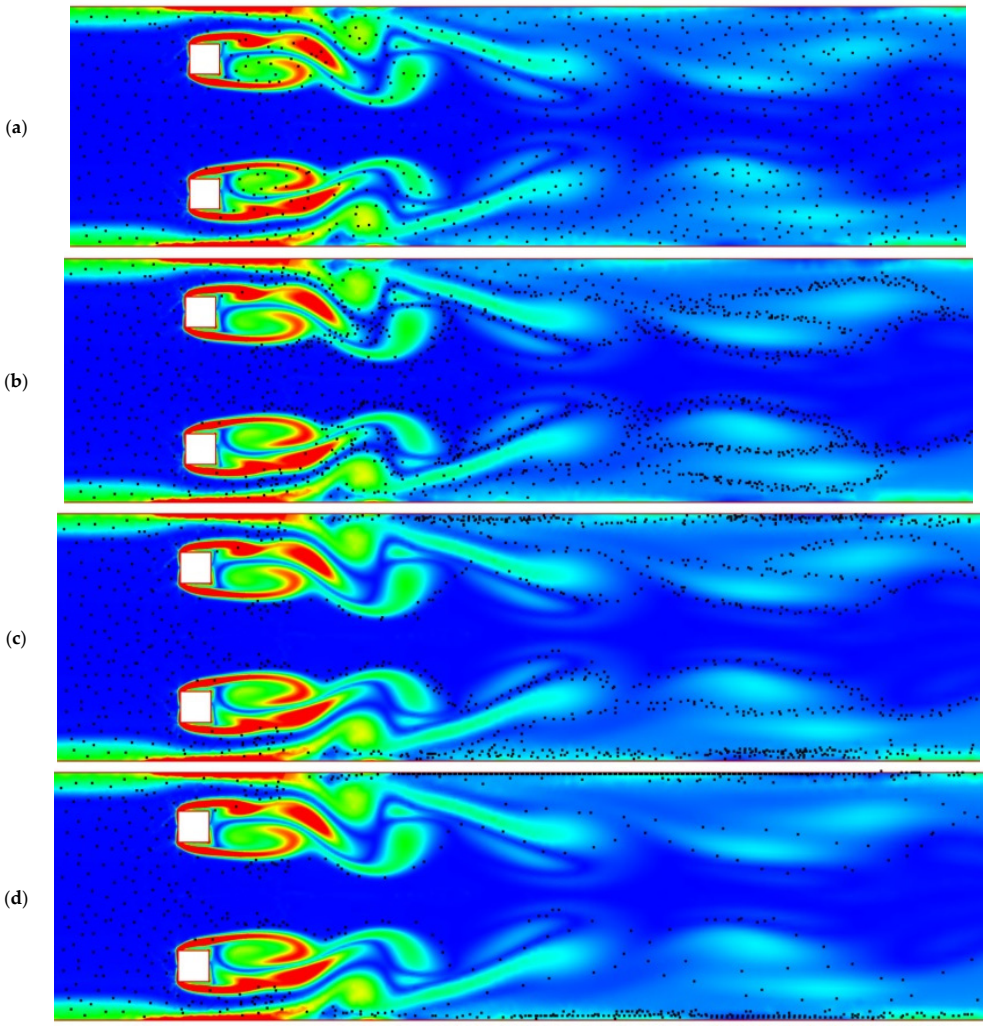

Figure 5. Dispersion of the particles inside the duct for (**a**) dp = 30 nm; (**b**) dp = 0.1 μm; (**c**) dp = 0.25 μm; (**d**) dp = 0.5 μm at Re = 100, S/D = 3.5, and Φ = 0.01.

Figure 6 discloses the concentration contours for different values of space ratio at Re = 100, d_p = 30 nm, and Φ = 0.01. It is observed that the concentrations of particles for all values of space

ratio are almost constant with a very low deposition near the duct surface for the regions before the obstacles. For these regions, the concentration for most parts of the duct keeps constant at the entrance concentration (Φ = 0.01). Note that the particles impacting to the duct walls bounce from the wall due to the reflect assumption of boundary but the flow. Moreover, thermophoretic force for the current case where the liquid temperature is higher than the wall temperature pushes the particles back toward the wall [37]. This causes a deposition of particles near the duct surface. This figure also discloses that the mass diffusion boundary layer is very narrow but is growing along the duct length. Finally, the particles concentration enhances in the recirculating wake region at the downstream of the obstacles. This means that the particles with this size are affected by the flow in the near wake region and some particles are distributed inside the vortex pathways.

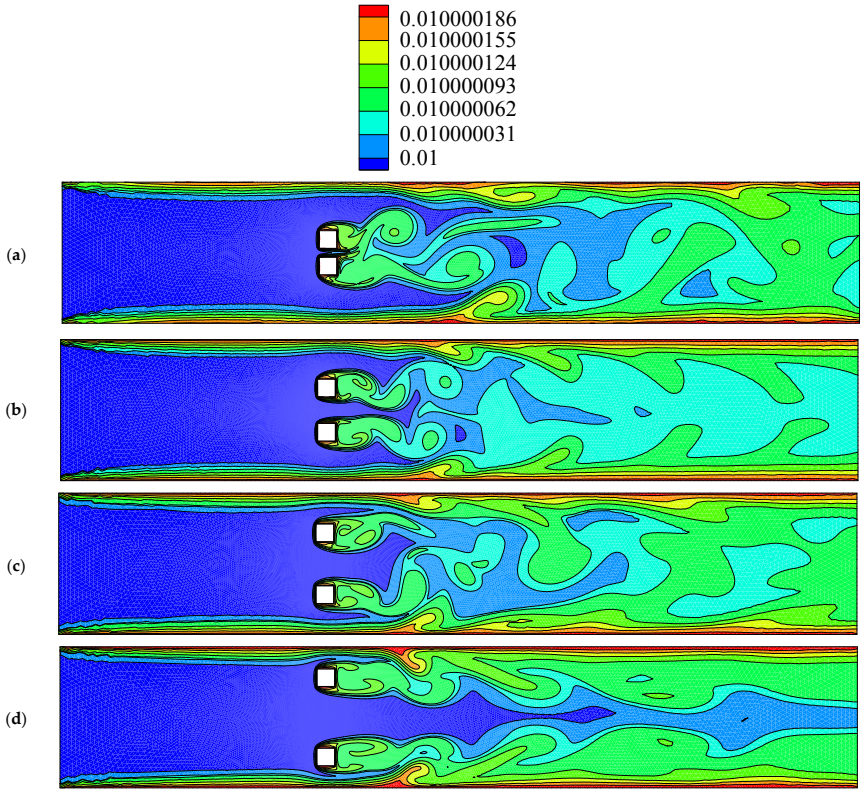

Figure 6. Concentration contours for (**a**) *S/D* = 1.5; (**b**) *S/D* = 2.5; (**c**) *S/D* = 3.5; (**d**) *S/D* = 4.5 at *Re* = 100, d_p =30 nm, and Φ = 0.01.

Effects of particle diameters on the particle deposition at *Re* = 100, Φ = 0.01, and *S/D* = 1.5 are disclosed in Figure 7. The deposition is defined as the ratio of the number of deposited particles on the all involved surfaces containing surfaces of obstacle and duct to the number of particles injected to the duct. It can be observed that the particle deposition enhances with an enhance in the particle diameter. This may be justified by the effect of gravity force on the particle deposition that becomes more significant for higher values of particle diameters. The particle deposition percentages are about 1.1%, 1.8%, 2.7%, and 4.6% for d_p = 30 nm, 0.1 µm, 0.25 µm, and 0.5 µm, respectively. Note that the trap boundary condition with a restitution coefficient of 0 is considered as the particle boundary condition on the surfaces of the duct and obstacles for evaluating particle deposition because for the reflect boundary, the particle deposition is zero as the restitution coefficient is equal to 1.

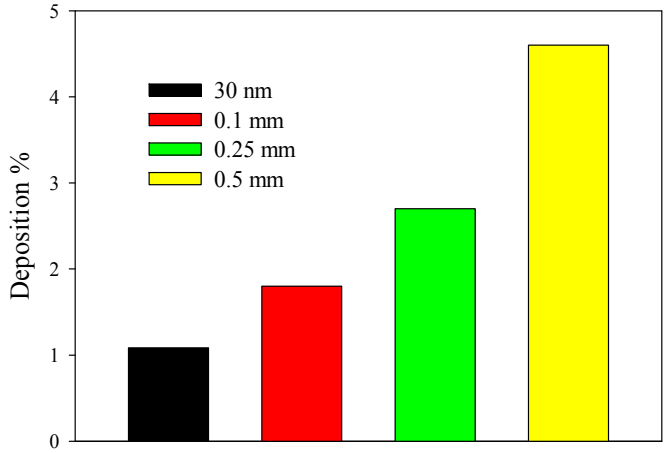

Figure 7. Particle deposition for different particle diameters at Re = 100, Φ = 0.01, and S/D = 1.5.

The effects of space ratio values on the particle deposition at Re = 100, Φ = 0.01, and d_p = 0.1 μm are disclosed in Figure 8. It is observed that the particle deposition enhances with an enhance in the value of space ratio. As mentioned earlier, the particles are affected by the flow in the near wake region for d_p = 0.1 μm. As the space ratio value increases, the distances between obstacles and duct walls decrease and the wake region of each obstacle transfers to the regions near the duct walls. Hence, the number of particles near the center of the duct reduces considerably and this leads to an increase in the number of particles that deposit on the duct's surfaces. The particle deposition percentages are about 1.8%, 2.3%, 3.1%, and 4.3% for S/D = 1.5, 2.5, 3.5, and 4.5, respectively.

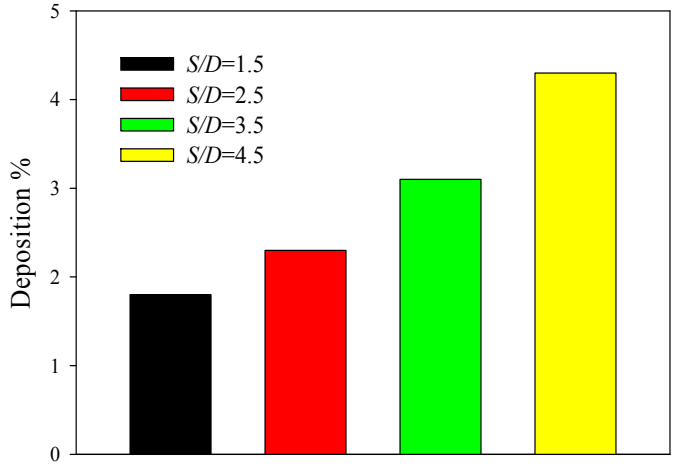

Figure 8. Particle deposition for different values of space ratio at Re = 100, Φ = 0.01, and d_p = 0.1 μm.

Figure 9 discloses the variations of mean Nusselt number on the top wall of the duct with different values of space ratio at Re = 100 and two values of volume fraction of nanoparticles. It can be observed that the mean Nusselt number enhances as the space ratio enhances. Generally, the heat transfer rate enhances by mounting the obstacle inside the duct because mixing of the hot liquid in center of the duct with cold liquid around the wall amends due to the oscillations generated by vortex shedding. As mentioned earlier, the distances between the walls of obstacles and duct decrease with an increase in the space ratio and accordingly, the oscillations generated by vortex shedding transfer to the regions around the duct walls. It worth noting that the fluid mixing near the duct wall increases with an increase in the space ratio, causing a higher temperature gradient around the duct wall and subsequently, a more efficient convection heat transfer. There are about 45% and 41% increments in the

mean Nusselt number for Φ = 0 and 0.01, respectively when the space ratio is increased in the range of 1–2.5. Finally, the mean Nusselt number enhances about 10% by using the particles in the liquid with Φ = 0.01 and d_p = 30 nm. This can be justified by positive effects of Brownian diffusion of particles and the drag of them on heat transfer improvement. Moreover, the thermal conductivity of nanofluid is more than that of the pure water case and this leads to a higher heat transfer rate.

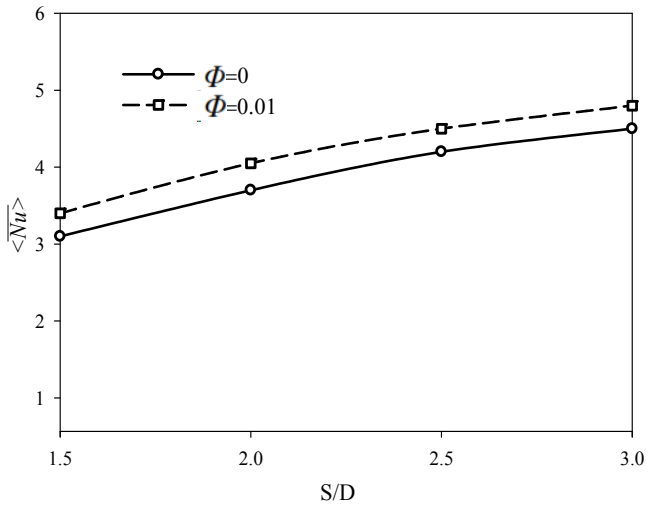

Figure 9. Variation of mean Nusselt number with space ratios for Re = 100, d_p = 30 nm, and two values of solid volume fraction of nanoparticles.

5. Conclusions

This paper used a two-way coupling of discrete phase model to track the discrete nature of aluminum oxide particles in an obstructed duct with two side-by-side obstacles. The effects of particle diameters and space ratios of obstacles on the dispersion and concentration of particles were evaluated. The obtained results showed that the particles with smaller diameter (d_p = 30 nm) are not affected by the flow streamline and they diffuse through the streamlines. However, the particles with larger diameters (i.e., 0.1 μm and 0.25 μm) accumulate in the vorticity regions around the perimeter of the vortices. It was concluded that the particle deposition increases with an increase in the particle diameter. The particle deposition percentages are about 1.1%, 1.8%, 2.7%, and 4.6% for d_p = 30 nm, 0.1 μm, 0.25 μm, and 0.5 μm, respectively. Moreover, about 45% and 41% increments in the mean Nusselt number were observed for Φ = 0 and 0.01, respectively when the space ratio is increased in the range of 1–2.5. Finally, it was found that the mean Nusselt number enhances about 10% by using the particles in the liquid with Φ = 0.01 and d_p = 30 nm.

Acknowledgments: R. Ellahi is grateful to PCST, Ministry of Science and Technology Pakistan to honed him with 5th top most Productive Scientist Award in category A in all subject for the year 2016.

Conflicts of Interest: The authors declare no conflict of interest.

References

1. Mahir, N.; Altaç, Z. Numerical investigation of convective heat transfer in unsteady flow past two cylinders in tandem arrangements. *Int. J. Heat Fluid Flow* **2008**, *29*, 1309–1318. [CrossRef]
2. Rashidi, M.M.; Abelman, S.; Freidoonimehr, N. Entropy generation in steady MHD flow due to a rotating porous disk in a nanofluid. *Int. J. Heat Mass Transf.* **2013**, *62*, 515–525. [CrossRef]
3. Sekrani, G.; Poncet, S. Further investigation on laminar forced convection of nanofluid flows in a uniformly heated pipe using direct numerical simulations. *Appl. Sci.* **2016**, *6*, 1–24. [CrossRef]
4. Vanaki, S.M.; Ganesan, P.; Mohammed, H.A. Numerical study of convective heat transfer of nanofluids: A review. *Renew. Sustain. Energy Rev.* **2016**, *54*, 1212–1239. [CrossRef]

5. He, Y.; Men, Y.; Zhao, Y.; Lu, H.; Ding, Y. Numerical investigation into the convective heat transfer of TiO_2 nanofluids flowing through a straight tube under the laminar flow conditions. *Appl. Therm. Eng.* **2009**, *29*, 1965–1972. [CrossRef]
6. Mirzaei, M.; Saffar-Avval, M.; Naderan, H. Heat transfer investigation of laminar developing flow of nanofluids in a microchannel based on Eulerian–Lagrangian approach. *Appl. Therm. Eng.* **2014**, *92*, 1139–1149. [CrossRef]
7. Bahremand, H.; Abbassi, A.; Saffar-Avval, M. Experimental and numerical investigation of turbulent nanofluid flow in helically coiled tubes under constant wall heat flux using Eulerian–Lagrangian approach. *Powder Technol.* **2015**, *269*, 93–100. [CrossRef]
8. Turki, S.; Abbassi, H.; Nasrallah, S.B. Two-dimensional laminar fluid flow and heat transfer in a channel with a built-in heated square cylinder. *Int. J. Therm. Sci.* **2003**, *42*, 1105–1113. [CrossRef]
9. Pirouz, M.M.; Farhadi, M.; Sedighi, K.; Nemati, H.; Fattahi, E. Lattice Boltzmann simulation of conjugate heat transfer in a rectangular channel with wall-mounted obstacles. *Sci. Iran. B* **2011**, *18*, 213–221. [CrossRef]
10. Heidary, H.; Kermani, M.J. Heat transfer enhancement in a channel with block(s) effect and utilizing Nano-fluid. *Int. J. Therm. Sci.* **2012**, *57*, 163–171. [CrossRef]
11. Mohyud-Din, S.T.; Khan, U.; Ahmed, N.; Hassan, S.M. Magnetohydrodynamic flow and heat transfer of nanofluids in stretchable convergent/divergent channels. *Appl. Sci.* **2015**, *5*, 1639–1664. [CrossRef]
12. Selimefendigil, F.; Öztop, H. Pulsating nanofluids jet impingement cooling of a heated horizontal surface. *Int. J. Heat Mass Transf.* **2014**, *69*, 54–65. [CrossRef]
13. Khan, W.; Gul, T.; Idrees, M.; Islam, S.; Khan, I.; Dennis, L.C.C. Thin filmWilliamson nanofluid flow with varying viscosity and thermal conductivity on a time-dependent stretching sheet. *Appl. Sci.* **2016**, *6*, 334. [CrossRef]
14. Sheikholeslami, M.; Ellahi, R. Electrohydrodynamic nanofluid hydrothermal treatment in an enclosure with sinusoidal upper wall. *Appl. Sci.* **2015**, *5*, 294–306. [CrossRef]
15. Akbar, N.S. Endoscopy analysis for the peristaltic flow of nanofluids containing carbon nanotubes with heat transfer. *Z. Naturforschung A* **2015**, *70*, 745–755. [CrossRef]
16. Selimefendigil, F.; Öztop, H. MHD mixed convection of nanofluid filled partially heated triangular enclosure with a rotating adiabatic cylinder. *J. Taiwan Inst. Chem. Eng.* **2014**, *45*, 2150–2162. [CrossRef]
17. Sheikholeslami, M.; Zia, Q.M.; Ellahi, R. Effect of induced magnetic field on free convective heat transfer of nanofluid considering KKL correlation. *Appl. Sci.* **2016**, *6*, 324. [CrossRef]
18. Bhatti, M.M.; Abbas, T.; Rashidi, M.M.; Ali, M.E.; Yang, Z. Entropy generation on MHD Eyring-Powell nanofluid through a permeable stretching surface. *Entropy* **2016**, *18*, 224. [CrossRef]
19. Mahian, O.; Kianifar, A.; Kalogirou, S.A.; Pop, I.; Wongwises, S. A review of the applications of nanofluids in solar energy. *Int. J. Heat Mass Transf.* **2013**, *57*, 582–594. [CrossRef]
20. Ahmad, S.; Rohni, A.M.; Pop, I. Blasius and sakiadis problems in nanofluids. *Acta Mech.* **2011**, *218*, 195–204. [CrossRef]
21. Shahmohamadi, H.; Rahmani, R.; Rahnejat, H.; Garner, C.P.; Balodimos, N. Thermohydrodynamics of lubricant flow with carbon nanoparticles in tribological contacts. *Tribol. Int.* **2016**. [CrossRef]
22. Shahmohamadi, H.; Rashidi, M.M. VIM solution of squeezing MHD nanofluid flow in a rotating channel with lower stretching porous surface. *Adv. Powder Technol.* **2016**, *27*, 171–178. [CrossRef]
23. Cheng, W.L.; Sadr, R. Induced flow field of randomly moving nanoparticles: A statistical perspective. *Microfluid Nanofluid* **2015**, *18*, 1317–1328. [CrossRef]
24. Bovand, M.; Rashidi, S.; Ahmadi, G.; Esfahani, J.A. Effects of trap and reflect particle boundary conditions on particle transport and convective heat transfer for duct flow—A two-way coupling of Eulerian–Lagrangian model. *Appl. Therm. Eng.* **2016**, *108*, 368–377. [CrossRef]
25. Bianco, V.; Chiacchio, F.; Manca, O.; Nardini, S. Numerical investigation of nanofluids forced convection in circular tubes. *Appl. Therm. Eng.* **2009**, *29*, 3632–3642. [CrossRef]
26. Talbot, L. Thermophoresis of particles in a heated boundary layer. *J. Fluid Mech.* **1980**, *101*, 737–758. [CrossRef]
27. Fluent Inc. *Fluent 6.2 User Manual*; Fluent Incorporated: Lebanon, NH, USA, 2006.
28. Minkowycz, W.J.; Sparrow, E.M.; Murthy, J.Y. *Handbook of Numerical Heat Transfer*, 2nd ed.; John Wiley & Sons: Hoboken, NJ, USA, 2006.

29. Garoosi, F.; Shakibaeinia, A.; Bagheri, G. Eulerian–Lagrangian modeling of solid particle behavior in a square cavity with several pairs of heaters and coolers inside. *Powder Technol.* **2015**, *280*, 239–255. [CrossRef]
30. Li, A.; Ahmadi, G. Dispersion and deposition of spherical particles from point sources in a turbulent channel flow. *Aerosol Sci. Technol.* **1992**, *16*, 209–226. [CrossRef]
31. Ounis, H.; Ahmadi, G.; McLaughlin, J.B. Brownian diffusion of submicrometer particles in the viscous sublayer. *J. Colloid Interface Sci.* **1991**, *143*, 266–277. [CrossRef]
32. Ranz, W.E., Jr.; Marshall, W.R. Evaporation from drops, Part I. *Chem. Eng. Prog.* **1952**, *48*, 141–146.
33. Fluent Inc. *FLUENT15 User Manual*; Fluent Incorporated: Lebanon, NH, USA, 2014.
34. Wu, C.L.; Berrouk, A.S. Discrete particle model for dense gas-solid flows. *Adv. Multiph. Flow Heat Transf.* **2012**, *3*, 151–187.
35. Patankar, S.V. *Numerical Heat Transfer and Fluid Flow*; Hemisphere: New York, NY, USA, 1980.
36. Heyhat, M.M.; Kowsary, F.; Rashidi, A.M.; Momenpour, M.H.; Amrollahi, A. Experimental investigation of laminar convective heat transfer and pressure drop of water-based Al_2O_3 nanofluids in fully developed flow regime. *Exp. Therm. Fluid Sci.* **2013**, *44*, 483–489. [CrossRef]
37. Rashidi, S.; Bovand, M.; Esfahani, J.A.; Ahmadi, G. Discrete particle model for convective Al_2O_3-water nanofluid around a triangular obstacle. *Appl. Therm. Eng.* **2016**, *100*, 39–54. [CrossRef]